PCCP

Cite this: *Phys. Chem. Chem. Phys.*, 2012, **14**, 1668–1676

www.rsc.org/pccp

PAPER

Synergistic reaction between SO_2 and NO_2 on mineral oxides: a potential formation pathway of sulfate aerosol†

Chang Liu, Qingxin Ma, Yongchun Liu, Jinzhu Ma and Hong He*

Received 6th July 2011, Accepted 14th September 2011
DOI: 10.1039/c1cp22217a

Sulfate is one of the most important aerosols in the atmosphere. A new sulfate formation pathway *via* synergistic reactions between SO_2 and NO_2 on mineral oxides was proposed. The heterogeneous reactions of SO_2 and NO_2 on CaO, α-Fe_2O_3, ZnO, MgO, α-Al_2O_3, TiO_2, and SiO_2 were investigated by *in situ* Diffuse Reflectance Infrared Fourier Transform Spectroscopy (*in situ* DRIFTS) at ambient temperature. Formation of sulfate from adsorbed SO_2 was promoted by the coexisting NO_2, while surface N_2O_4 was observed as the crucial oxidant for the oxidation of surface sulfite. This process was significantly promoted by the presence of O_2. The synergistic effect between SO_2 and NO_2 was not observed on other mineral particles (such as $CaCO_3$ and $CaSO_4$) probably due to the lack of the surface reactive oxygen sites. The synergistic reaction between SO_2 and NO_2 on mineral oxides resulted in the formation of internal mixtures of sulfate, nitrate, and mineral oxides. The change of mixture state will affect the physicochemical properties of atmospheric particles and therefore further influence their environmental and climate effects.

1. Introduction

As a major constituent of atmospheric particulate matter, sulfate accounts for the largest mean mass fraction of both fine and coarse aerosol particles.[1] In the atmosphere, sulfate aerosols can be transported several thousand kilometres and can have a mean lifetime of about one week.[2,3] They can produce a cooling effect on the global climate by scattering solar radiation (direct effect)[4–6] and can also act as cloud condensation nuclei (indirect effect).[7–12] The global average direct forcing of sulfate aerosols ranges from -0.26 W m^{-2} to -0.82 W m^{-2}, while indirect forcing on cloud albedo varies from -0.3 W m^{-2} to -1.8 W m^{-2},[13] indicating their competitive effect on the climate with greenhouse gases (1.5 W m^{-2} for CO_2 and 0.95 W m^{-2} for other greenhouse gases[14]). Additionally, sulfate derived from anthropogenic emissions of SO_2 is a major contributor to the acidity of rainwater, giving rise to the severe environmental problem of acidification.[15] On account of its key role in the global climate and air quality, the formation mechanism of sulfate is a pressing environmental concern.

Atmospheric secondary sulfate aerosols form by the oxidation of SO_2 either in gaseous phase reactions with hydroxyl radicals followed by condensation of sulfuric acid (*e.g.* reactions (1) and (2)), or in aqueous phase reactions within cloud and fog droplets (*e.g.* reaction (3) or (4)).[7]

$$SO_2 + OH + O_2 \rightarrow SO_3 + HO_2 \quad (1)$$

$$SO_3 + H_2O \rightarrow H_2SO_4 \quad (2)$$

$$SO_3^{2-} + O_3 \rightarrow SO_4^{2-} + O_2 \quad (3)$$

$$HSO_3^- + H_2O_2 \rightarrow HSO_4^- + H_2O \quad (4)$$

However, large uncertainties still remain concerning the mechanism of sulfate formation. A number of models have been applied to predict the formation of sulfate on a global scale. Results have shown that SO_2 concentration is typically overestimated while sulfate concentration tends to be underestimated.[16] Therefore, there must be some yet unknown pathways for the conversion of SO_2 to sulfate aerosols.

Recently, heterogeneous oxidation of SO_2 on the surface of mineral dust particles was investigated, showing that adsorption of SO_2 only leads to sulfite or bisulfite on the surface of mineral oxides.[17–19] Oxidants, such as O_3, are needed in the conversion of sulfite to sulfate.[20] In addition, NO_2, which is an important atmospheric pollutant with similar anthropogenic sources as SO_2, provides a promotive effect on the absorption and oxidation of SO_2 in flue gas desulfurization with high gaseous pollutant concentration and a reaction temperature of 423 K.[21] Previous studies have also found that the formation of sulfate was enhanced by NO_2 on Sahara Desert mineral dust under ambient conditions.[22] However, the interaction mechanism between SO_2 and NO_2 remains unclear. In our previous work,[23]

Research Center for Eco-Environmental Sciences, Chinese Academy of Sciences, Beijing, 100085, China. E-mail: honghe@rcees.ac.cn; Fax: +86-10-6292-3563; Tel: +86-10-6284-9123
† Electronic supplementary information (ESI) available. See DOI: 10.1039/c1cp22217a

we found that a synergistic effect existed in the heterogeneous reaction between SO_2 and NO_2 on γ-Al_2O_3. Since mineral dust originates from wind-blown soils, its chemical composition is similar to that of crustal rock.[24] Besides Al_2O_3, the earth's crust is also dominated by other oxides such as SiO_2, CaO, and α-Fe_2O_3. However, the applicability of synergistic reactions between SO_2 and NO_2 on other mineral oxides is not known.

In the present study, heterogeneous reactions of SO_2 and NO_2 on typical mineral oxides (CaO, α-Fe_2O_3, ZnO, MgO, α-Al_2O_3, TiO_2, and SiO_2) were investigated using *in situ* Diffuse Reflectance Infrared Fourier Spectroscopy (*in situ* DRIFTS). The synergistic effect on the formation of sulfate was further elucidated. In addition, the difference in the heterogeneous reactions of SO_2 and NO_2 between mineral oxides and other typical atmospheric particles was compared. The aim of this work was to give an insight into the complex atmospheric chemistry of SO_2, NO_2, and atmospheric particles.

2. Experimental section

2.1 Sample preparation and characterization

The following mineral oxide particles were used in this study: CaO, α-Fe_2O_3, ZnO, MgO, α-Al_2O_3, TiO_2, and SiO_2. The α-Al_2O_3 particles were prepared from boehmite (AlOOH, Shandong Aluminum Corporation) by calcining at 1473 K for 180 min. All other oxide particles were purchased from commercial sources. The BET surface areas were characterized by a physisorption analyzer (Autosorb-1C-TCD, Quantachrome) and sample particle sizes were measured by transmission electron microscopy (TEM, H-7500, Hitachi). The characterization results are listed in Table 1.

In addition to the mineral oxides listed in Table 1, other typical atmospheric particles, $CaCO_3$ (AR, Sinopharm Chemical Reagent Co. Ltd, China) and $CaSO_4$ (AR, Sinopharm Chemical Reagent Co. Ltd, China), were chosen as the representatives of other mineral particles. All these particles were used as purchased.

2.2 *In situ* DRIFTS measurements

The heterogeneous reactions of SO_2 and NO_2 on particles were measured by *in situ* DRIFTS (NEXUS 670, Thermo Nicolet Instrument Corporation), equipped with an *in situ* diffuse reflection chamber and a high-sensitivity mercury cadmium telluride (MCT) detector cooled by liquid N_2. Before the experiment, oxide samples were finely ground and placed into a ceramic crucible in the *in situ* chamber. In order to remove the adsorbed species (*e.g.* CO_2 and H_2O) on the surface, the samples were first pretreated at 573 K for 180 min in a stream of synthetic air (80% N_2 and 20% O_2) in a total flow of 100 mL min^{-1}. After 60 min the temperature was cooled to room temperature (303 K) and the samples were exposed to 200 ppmv SO_2 and/or 200 ppmv NO_2 balanced with 100 mL min^{-1} synthetic air for at least 120 min. All reactive and carrier gases are of high-purity (99.999%) in our study to ensure the absence of impurities (such as CO_2). The infrared spectra were collected using a computer with OMNIC 6.0 software (Nicolet Corporation, USA). All spectra were recorded at a resolution of 4 cm^{-1} for 100 scans in the spectral range of 600 to 4000 cm^{-1}. The low frequency cutoff of spectra was due to the strong lattice oxide absorption of the samples.

Table 1 Characterizations of mineral oxide particles used

Mineral oxide	Commercial source	Average particle size/nm	Surface area/m^2 g^{-1}
CaO	Shantou Xilong Chemistry Factory	1300	6.1
α-Fe_2O_3	Shantou Xilong Chemistry Factory	87	2.6
ZnO	Shantou Xilong Chemistry Factory	204	1.8
MgO	Shantou Xilong Chemistry Factory	1000	14.6
α-Al_2O_3	AlOOH, 1473 K, 180 min	1000	12.0
TiO_2	Degussa	25	50
SiO_2	Degussa	20	230

3. Results and discussion

3.1 Synergistic effect between SO_2 and NO_2 on CaO

Firstly, the heterogeneous reaction of SO_2 and NO_2 on CaO was investigated. The pretreated sample was exposed to SO_2 and NO_2 balanced with synthetic air in a total flow of 100 mL min^{-1} at 303 K. The *in situ* DRIFTS spectra as a function of time are shown in Fig. 1. At the beginning of the reaction, several bands at 1000, 940, 895, and 850 cm^{-1} were observed in the spectra. The bands at 940 and 850 cm^{-1} are attributed to the symmetric stretching of monodentate sulfite, while bands at 1000 and 895 cm^{-1} are assigned to the asymmetric stretching vibration of monodentate sulfite.[25] As the reaction proceeded, these absorption features of sulfite decreased while bands at 1192, 1140, and 1099 cm^{-1} increased. These bands could be assigned to the asymmetric vibration frequency of bidentate surface-coordinated sulfate.[26,27] The symmetric stretching of sulfate at 950–1000 cm^{-1} was overlapped by the absorption of sulfite.[28] The increase of sulfate species as well as the decrease of sulfite species made it difficult to distinguish the absorption bands in this region of the spectra. Nevertheless, the results indicate that surface sulfite was converted to sulfate in the reaction process. In addition, the bands at 1638, 1519, 1336, and 815 cm^{-1} grew with increased exposure time, which was attributed to the presence of nitrate species on the CaO surface. The band at 1519 cm^{-1} is assigned to the asymmetric stretching

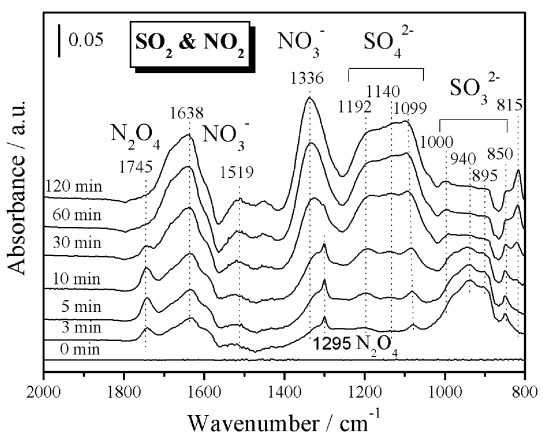

Fig. 1 Dynamic changes in the *in situ* DRIFTS spectra of the CaO sample as a function of time with a flow of 200 ppmv SO_2 + 200 ppmv NO_2 + 20% O_2 + 80% N_2 at 303 K. Total flow rate was 100 mL min^{-1}.

mode of monodentate nitrate,[29] while the bands at 1638 and 815 cm^{-1} are attributed to the asymmetric stretching and out-of-plane bend of bridging nitrate, respectively.[30] Due to remnant water in the feed gas at room temperature, the water-solvated surface nitrate with asymmetric stretching mode at 1336 cm^{-1} appeared and acted as the dominant nitrate on the CaO surface.[30] The symmetric stretching region of the surface nitrate (1000–1050 cm^{-1}) was overlapped by strong sulfate absorption (1000–1200 cm^{-1}),[25] which was difficult to indicate in Fig. 1. In addition, two peaks at 1745 and 1295 cm^{-1} rapidly increased at the early stage of the reaction, then decreased in intensity as the reaction progressed. These two peaks are assigned to the asymmetric and symmetric stretching of the dimer of NO_2, namely N_2O_4, respectively.[31–33] The reaction behavior of N_2O_4 suggested it was an intermediate species in the synergistic reaction between SO_2 and NO_2.

Further quantitative analysis of surface species was conducted by integrating the absorbance band areas. As shown in Fig. 2, sulfite and N_2O_4 species were dominant at the initial stage of the reaction, and reached maximum at 3 min and then gradually decreased to zero after 40 min. Additionally, a dramatic increase in sulfate species was observed after 3 min reaction, and it steadied after 40 min. It seems that the consumption of sulfite and N_2O_4 accompanied the formation of sulfate. As for the formation of nitrate, the formation rate remained steady during the reaction.

In situ DRIFTS spectra of CaO exposed to individual SO_2 or NO_2 with synthetic air are displayed in Fig. 3a and b, respectively. For SO_2 adsorption (Fig. 3a), formation of sulfite dominated the surface reaction and resulted in the broad band centered at 943 cm^{-1}. This band is attributed to the stretching mode of monodentate sulfite species.[19] The broad band at 1647 cm^{-1} is assigned to δ(HOH) vibration of molecularly adsorbed water.[30,34] The flow of SO_2 + air was switched to only air for 60 min to flush the surface; however, peak intensity of sulfite remained unchanged. This indicated that SO_2 was chemisorbed on the surface. Further adsorption of NO_2 on the SO_2 pre-saturated CaO surface was conducted and the spectra are shown in Fig. 3a. As the exposure time increased, the sulfite

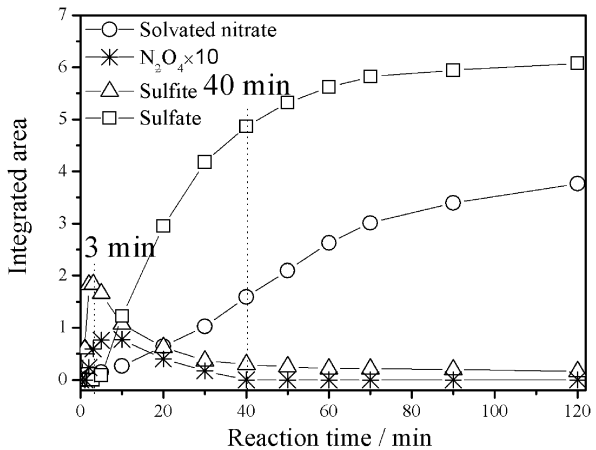

Fig. 2 Dynamic changes of integrated absorbance area for N_2O_4 (1745 cm^{-1}), sulfite (900–1000 cm^{-1}), sulfate (1100–1200 cm^{-1}), and water-solvated nitrate (1336 cm^{-1}) observed during the reaction of SO_2 and NO_2 on CaO (as shown in Fig. 1).

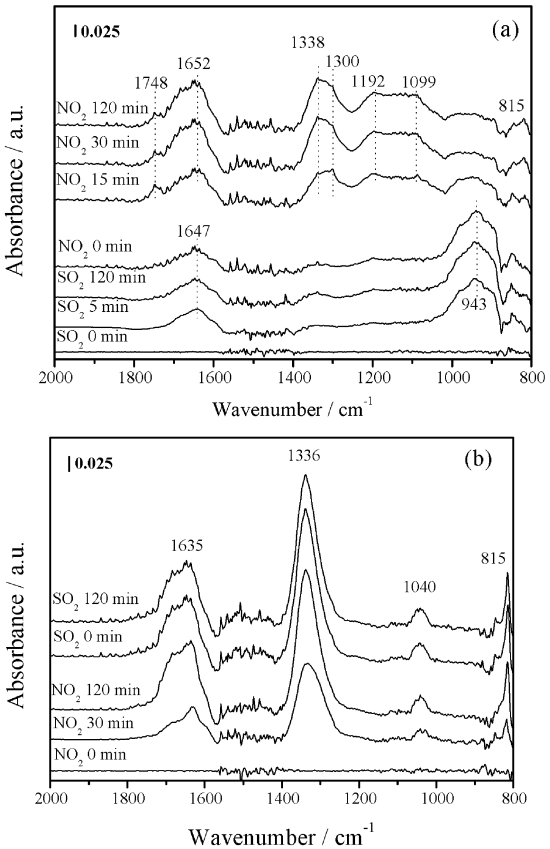

Fig. 3 *In situ* DRIFTS spectra of (a) 200 ppmv SO_2 reaction on CaO surface followed by 200 ppmv NO_2 reaction; (b) 200 ppmv NO_2 reaction on CaO surface followed by 200 ppmv SO_2 reaction as a function of time in a flow of 100 mL min^{-1} synthetic air (20% O_2, 80% N_2) at 303 K.

species band at 943 cm^{-1} gradually decreased while the sulfate bands at 1099 and 1192 cm^{-1} increased. In addition, the features of N_2O_4 at 1748 and 1300 cm^{-1} appeared at the early stage of the reaction but decreased in intensity with increasing reaction time. This implied that N_2O_4 played a crucial role in the oxidation of surface sulfite to sulfate. Peaks due to bridging (1652, 815 cm^{-1}) and water-solvated (1338 cm^{-1}) nitrate were also detected on the CaO surface after SO_2 pre-saturation.

In the case of NO_2 adsorption (Fig. 3b), the intensities of bands at 1635, 1336, 1040, and 815 cm^{-1} increased with reaction time. The most prominent band at 1336 cm^{-1} is assigned to water-solvated nitrate.[30] Absorption peaks at 1635, 1040, and 815 cm^{-1} are attributed to asymmetric stretching, symmetric stretching, and out-of-plane mode of bridging nitrate, respectively.[30] After saturation with nitrate species, the surface was purged by synthetic air for 60 min and was then exposed to SO_2 for 120 min, but no spectral change was observed.

To illuminate the synergistic effect between SO_2 and NO_2 on the formation of surface species, the integrated areas of sulfate, sulfite, bridging nitrate, and solvated nitrate formed on CaO under different reaction conditions were compared and are shown in Fig. 4. Compared with the individual reaction of SO_2, formation of sulfate was significantly promoted (Fig. 4a) while sulfite was quickly consumed (Fig. 4b) in the presence of NO_2. As for nitrate, the presence of SO_2 had no influence on the generation of bridging nitrate (Fig. 4c), but the formation

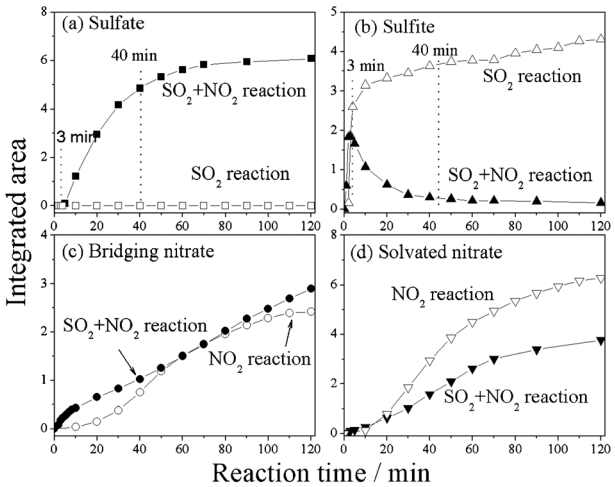

Fig. 4 Comparison of the integrated area of (a) sulfate (1100–1200 cm^{-1}), (b) sulfite (900–1000 cm^{-1}), (c) bridging nitrate (1638 cm^{-1}), and (d) solvated nitrate (1336 cm^{-1}) formed under different reaction conditions. Solid points: SO_2 and NO_2 simultaneous reaction (Fig. 1); hollow points: SO_2 individual reaction (Fig. 3a) or NO_2 individual reaction (Fig. 3b).

of solvated nitrate was significantly reduced by the coexisting SO_2 (Fig. 4d). By measuring the apparent single-hygroscopicity parameter (κ), it is established that the hygroscopicity of insoluble $CaSO_4$ ($\kappa = \sim 0.001$) is much less hygroscopic than that of soluble $Ca(NO_3)_2$ ($\kappa = \sim 0.5$).[35] Therefore, the formation of less hygroscopic $CaSO_4$ resulted in a decrease in surface water, which consequently reduced the formation of water-solvated nitrate species. These results demonstrated that the reaction behaviors of SO_2 and NO_2 on the CaO surface were influenced by the synergistic effect between them.

3.2 Synergistic effect between SO_2 and NO_2 on other typical mineral oxides

To clarify the synergistic reaction between SO_2 and NO_2 on other mineral oxides, *in situ* DRIFTS experiments were carried out with SO_2 and NO_2 introduced simultaneously or individually onto other mineral oxides. The surface species formed during the reaction are summarized in Table 2. The integrated area of surface species was compared, as shown in Fig. 5. When SO_2 was individually introduced into the reaction system with synthetic air, sulfite was the only surface species observed on ZnO and TiO_2, while weakly adsorbed SO_2 formed on α-Al_2O_3. For MgO, in addition to sulfite, the absorption band at 1150 cm^{-1} corresponding to the asymmetric stretching of sulfate was detected, which is in agreement with previous research.[19] When SO_2 and NO_2 coexisted in the reaction gases, generation of sulfite was obviously reduced while the formation of sulfate was significantly promoted on the surface of these oxides. Therefore, oxidation of SO_2 to sulfate in the presence of NO_2 at room temperature was a common phenomenon on these mineral oxides. In addition, water-solvated nitrate was the major surface nitrate species on these oxides when NO_2 was introduced on its own. Similar to CaO, the decrease in surface water caused by the generation of less hygroscopic sulfate resulted in a reduction in the formation of solvated nitrate. In our previous study, the enhancement of sulfate formation as well as inhibition of nitrate generation were observed in the synergistic reaction between SO_2 and NO_2 on γ-Al_2O_3.[23] In addition to N_2O_4, nitrite (NO_2^-) was also observed as an intermediate species for the formation of nitrate. Nitrite was not detected on the oxides such as α-Al_2O_3 in this study, however, which likely resulted from the differences in the formation rate and further oxidation rate of the surface intermediate between different oxides.

The case of α-Fe_2O_3 was slightly different since α-Fe_2O_3 is more active than other oxides in the oxidation of SO_2 to sulfate. Previous research has shown that adsorbed SO_2 can be oxidized to surface sulfate species on α-Fe_2O_3 at ambient temperatures.[40] In the current work, bridging (1628, 1240 cm^{-1}), bidentate (1602, 1288 cm^{-1}), and monodentate (1580 cm^{-1}) nitrates were observed when NO_2 was individually introduced into the system (Fig. 6a).[28,38,39] When α-Fe_2O_3 was exposed to SO_2, bands were detected at 1270, 1161, and 1101 cm^{-1}, which corresponded to the asymmetric stretching of sulfate (Fig. 6b)[30] and indicated the direct formation of sulfate from SO_2 on α-Fe_2O_3. Compared with the simultaneous reaction of SO_2 and NO_2 (Fig. 6c), however, the generation of sulfate was still obviously promoted in the presence of NO_2 (Fig. 6d). The similarity in the reaction behaviors of SO_2 and NO_2 on ZnO, TiO_2, α-Al_2O_3, MgO, α-Fe_2O_3, and CaO implied that the mechanism of synergistic reactions on these mineral oxides was identical.

In situ DRIFTS spectra of the SO_2 and NO_2 reaction on SiO_2 are shown in Fig. 7. Peaks were observed at 1675, 1626, 1416, 1346, and 1267 cm^{-1} in the spectra. The band at 1626 cm^{-1} was due to surface adsorbed water originating from remnant water in the feed gas. The bands at 1346, 1416, and 1675 cm^{-1} that correspond to the bending mode of $\nu_s(NO_2)$, $\delta(OH)$, and $\nu_a(NO_2)$ indicated the formation of adsorbed HNO_3 on the SiO_2 surface.[32] Vibration mode $\delta(HON)$ at 1267 cm^{-1} was observed, implying the possible formation of HONO in the reaction.[31,32] These results suggest that the reaction of NO_2 with surface water was dominant on the SiO_2 surface. Due to the inhibition of SO_2 adsorption, formation of sulfate was not observed when NO_2 was present in the system. This is expected because SiO_2 is an acidic oxide and not reactive to acidic SO_2 and NO_2. Therefore, surface nitrate and sulfate are hardly to form on SiO_2.

3.3 Comparison of reactivity between mineral oxides and other atmospheric particles

The formation of sulfate due to the synergistic reaction between SO_2 and NO_2 was demonstrated on mineral oxides. To determine whether this effect occurred on other mineral particulate matters, the reactions of SO_2 and NO_2 on $CaCO_3$ and $CaSO_4$ were also tested. No surface reaction of SO_2 and NO_2 was observed on these particles (as seen from Fig. S1, ESI†). The difference between mineral oxides and other mineral particles on the reactivity of SO_2 and NO_2 was ascribed to their distinctive surface properties.

3.4 Possible mechanism of synergistic effect

The surface reaction mechanism of SO_2 is different from that of NO_2 on metal oxides.[25] Initially, NO_2 adsorbs on metal sites of metal oxide particles (for example, γ-Al_2O_3, α-Al_2O_3, Fe_2O_3, and TiO_2) to form nitrite and then nitrate *via* reaction with

Table 2 Assignment of vibrational bands (cm^{-1}) of surface species formed when mineral oxides were simultaneously exposed to SO_2 and NO_2

Surface species	Representation	CaO	α-Fe_2O_3	ZnO	TiO_2	MgO	α-Al_2O_3
Monodentate nitrate		1519[30]	1580[30]	1521[30]	1450,[36] 1500[36]	1460[30]	1540[29,30]
Bidentate nitrate	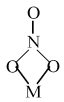		1288,[37] 1602[30]	1568[30]	1585[30,38]		1585[30]
Bridging nitrate	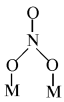	815,[30] 1638[30]	1240,[30] 1628[30]	1625[30]	1244,[37,38] 1624[30,38]	1640,[30] 1024[30]	1626[29,30]
Water-solvated nitrate	NO_3^- (aq)	1336[30]	1338[30]	1299[30]	1300,[37] 1330[30]	1310[30]	1317,[30] 1344[29]
N_2O_4	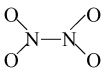	1295,[32,33] 1745[32,33]	1300,[32,33] 1749[32,33]	1300,[32,33] 1747[32,33]	1300,[32,33] 1747[32,33]	1298,[32,33] 1731[32,33]	1740[32,33]
Physically adsorbed SO_2	$SO_{2(ad)}$						1137[19,26]
Monodentate sulfite	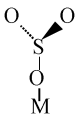	850,[22,25] 895,[22,25] 940,[22,25] 1000[22,25]		955,[28,39] 1002,[28,39] 1057[28,39]	1070[28,39]	1030,[19,26] 990[19,26]	
Bridging sulfate	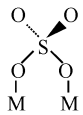			1140,[28,39] 1189[28,39]	1105,[28,39] 1140,[28,39] 1170[28,39]		1260[19,26]
Bidentate sulfate	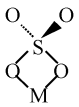	1099,[19,26] 1140,[19,26] 1192[19,26]	1036,[40] 1097,[40] 1160,[40] 1268[40]			1165,[19,26] 1150[19,26]	

The superscript numbers are the sequence numbers of corresponding references.

another nitrite in an Langmuir–Hinshelwood (LH) type mechanism or with NO_2 in an Eley–Rideal (ER) type mechanism.[37,41] In the reactions shown below, M represents a metal atom of the oxides surface:

$$NO_{2(g)} + M \rightarrow MNO_2 \quad (5)$$

$$2MNO_2 \rightarrow MNO_3 + NO_{(g)} \quad (6)$$

$$MNO_2 + NO_{2(g)} \rightarrow MNO_3 + NO_{(g)} \quad (7)$$

For SO_2 adsorption on metal oxide surfaces, surface-coordinated sulfite/bisulfite forms on basic oxide anions (oxygen atoms or adsorbed hydroxyl), while weakly adsorbed SO_2 forms on acidic metal sites.[19] Previous studies have proposed SO_2 as an electron acceptor on metal oxides (MgO, Al_2O_3, ZrO_2, TiO_2, and CeO_2) through adsorption on either surface oxygen sites to form strongly adsorbed sulfite species or on basic hydroxyl groups leading to the formation of hydrogen-sulfite species.[42]

In the present work, surface oxygen sites and hydroxyl groups contributed to SO_2 adsorption, while metal sites were the adsorption sites for NO_2. In some cases, the consumption of surface hydroxyl groups was not observed (*e.g.* CaO, Fig. S2, ESI†). Therefore, the number of surface oxygen sites may play a key role in the reaction.

It is proposed that gases such as O_2 adsorb on the surface of oxides and produce surface active oxygen species.[43] Oxygen is also a key reactant in the oxidation of adsorbed SO_2 on the surface of iron oxides to form surface sulfate species at ambient temperatures.[40] To explore the role of O_2 in the synergistic reaction between SO_2 and NO_2, an experiment without O_2 was carried out by exposing CaO to SO_2 and NO_2 in a 100 mL min^{-1} N_2 flow. As is displayed in Fig. 8, peaks at 1624, 1581, 1322, 1035, 850, and 817 cm^{-1} were observed after 600 min, which were quite different from those obtained in the presence of O_2 (Fig. 1). In the initial 180 min reaction, the formation of surface bidentate nitrite species (1230 cm^{-1}) dominated the surface reaction.[44] This suggested that the reactivity of SO_2 and NO_2 decreased in the absence of O_2. Conversion of nitrite to water-solvated nitrate (1322 cm^{-1}), bidentate nitrate (1581 cm^{-1}), and bridging nitrate (817, 1035, and 1624 cm^{-1}) was observed as exposure time increased,[30] which implied that nitrite was the intermediate of NO_2 to nitrate. These results are consistent with previous studies.[37] Sulfite at 850 cm^{-1} was detected in the spectra until 120 min.[43] However, the formation

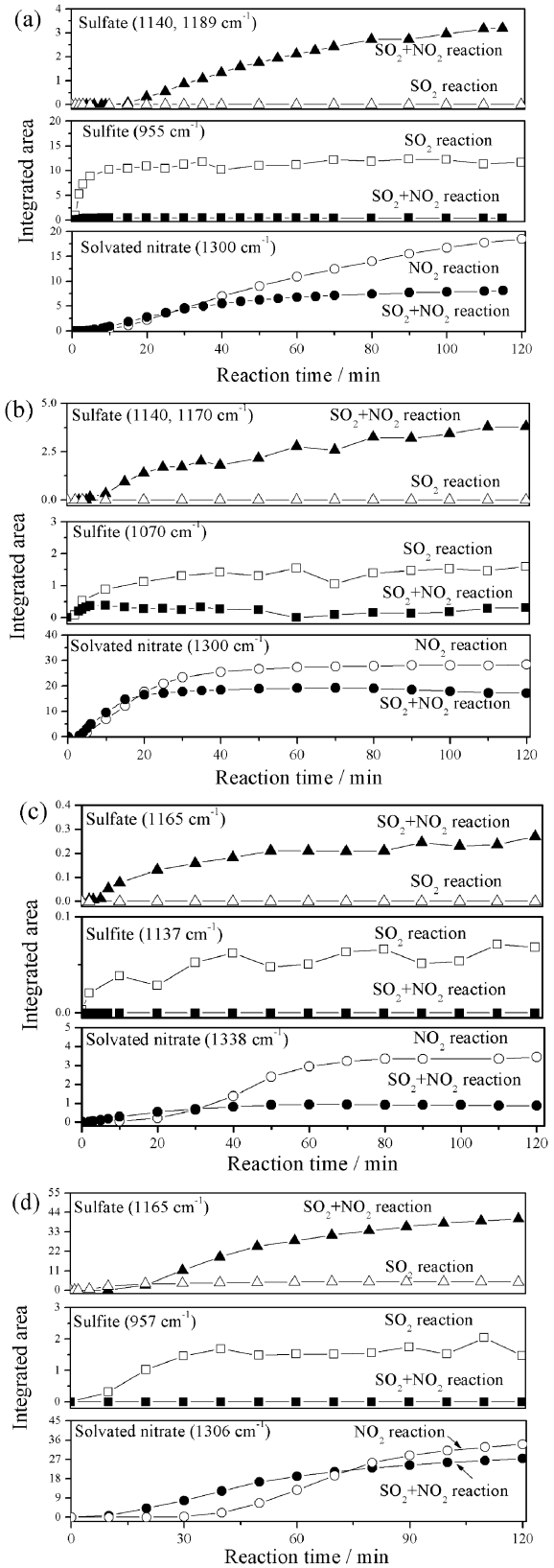

Fig. 5 Comparison of the integrated area of surface species between 200 ppmv NO_2 and 200 ppmv SO_2 simultaneous reaction (solid points) and 200 ppmv SO_2 or 200 ppmv NO_2 individual reaction (hollow points) on (a) ZnO, (b) TiO_2, (c) α-Al_2O_3, and (d) MgO.

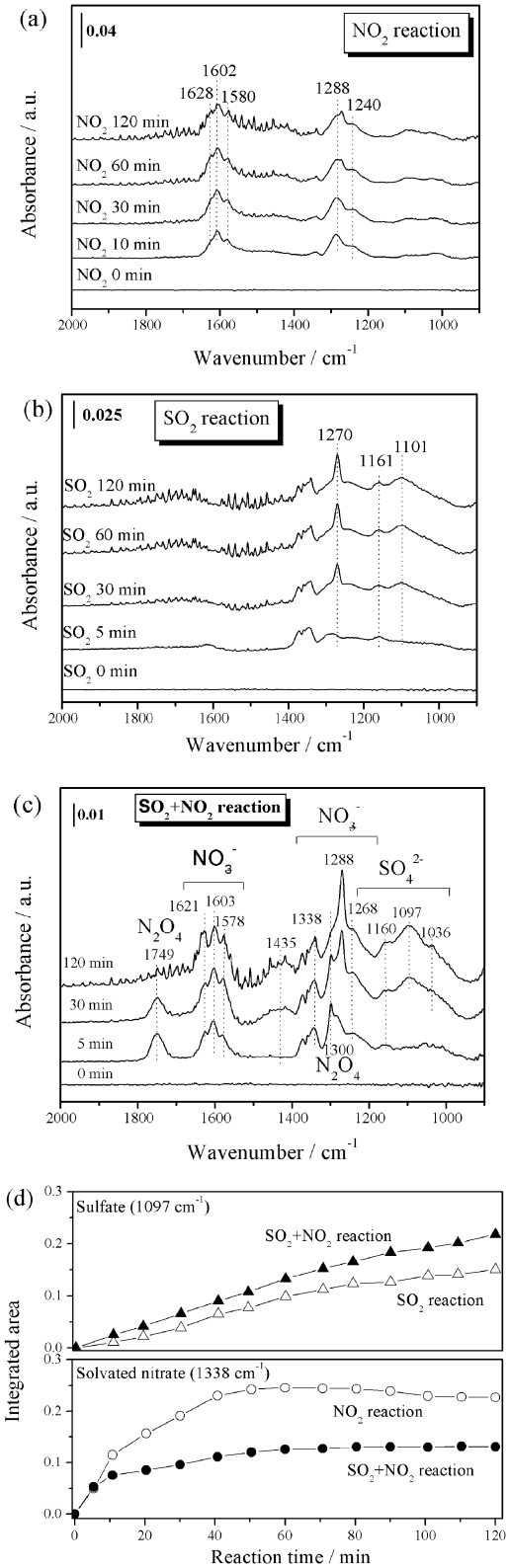

Fig. 6 *In situ* DRIFTS spectra of (a) 200 ppmv SO_2 reaction, (b) 200 ppmv NO_2 reaction, and (c) SO_2 and NO_2 simultaneous reaction on the surface of α-Fe_2O_3 as a function of time in a flow of 100 mL min^{-1} synthetic air (20% O_2, 80% N_2) at 303 K; (d) comparison of the integrated area of surface species between SO_2 and NO_2 simultaneous reaction (solid points) and SO_2 or NO_2 individual reaction (hollow points) on α-Fe_2O_3.

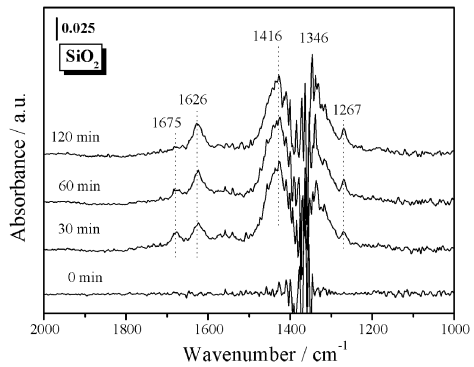

Fig. 7 *In situ* DRIFTS spectra of 200 ppmv SO_2 and 200 ppmv NO_2 reaction on the surface of SiO_2 as a function of time in a flow of 100 mL min^{-1} synthetic air (20% O_2, 80% N_2) at 303 K.

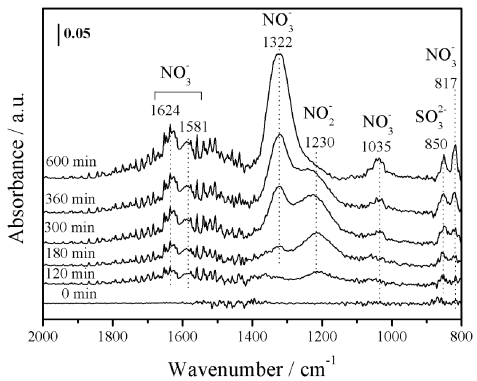

Fig. 8 *In situ* DRIFTS spectra of 200 ppmv SO_2 and 200 ppmv NO_2 reaction on the surface of CaO in 100 mL min^{-1} N_2 flow as a function of time at 303 K.

of both sulfate and N_2O_4 were not detected even as the reaction continued to 600 min, which demonstrated that the interaction between N_2O_4 and sulfite was necessary for the formation of sulfate. As discussed above, surface oxygen sites contributed to the adsorption of SO_2. By providing abundant surface oxygen sites for initial adsorption of SO_2, oxygen played a crucial role in the formation of sulfate. However, O_2 was not considered as the direct oxidant of adsorbed SO_2 as no oxidation of sulfite occurred on the mineral oxides (except α-Fe_2O_3) when SO_2 was introduced into the system in the presence of O_2. In addition, as seen in Fig. 1 and 8, surface N_2O_4 was also promoted by the presence of O_2, which implied oxygen might also induce the formation of N_2O_4, although the mechanism remains unclear.

Since nitrite, nitrate, and N_2O_4 all coexisted with sulfite during the simultaneous reaction of SO_2 and NO_2, all were possible oxidants for the conversion of sulfite to sulfate. As there was no formation of sulfate when nitrite and nitrate coexisted with sulfite (Fig. 8), neither species were relevant to SO_2 oxidation. It is known that N_2O_4 could isomerize and autoionize to $NO^+NO_3^-$ in solution or at low temperatures,[33,45,46] and can rapidly oxidize many organic and inorganic compounds.[45] Therefore, N_2O_4 was considered the oxidant for the formation of sulfate in this work.

The reaction mechanism proposed for the synergistic effect between SO_2 and NO_2 on mineral oxides is illustrated in Scheme 1. Firstly, gaseous NO_2 and SO_2 adsorb on the surface

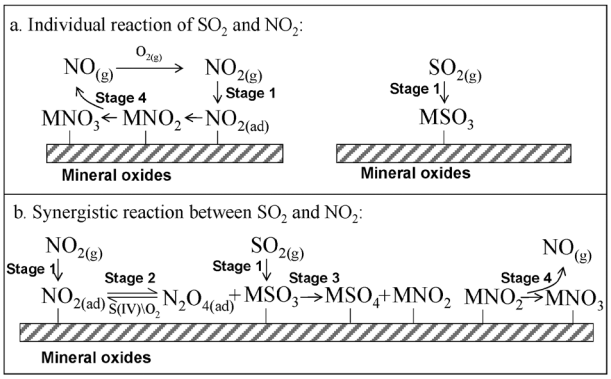

Scheme 1 Reaction mechanism proposed for the synergistic reaction between SO_2 and NO_2.

to form adsorbed $NO_{2(ad)}$ and sulfite, respectively, and $NO_{2(ad)}$ dimerizes to $N_2O_{4(ad)}$. The identification of active sites for N_2O_4 formation is difficult at present. Since Henry's law coefficient for N_2O_4 in water is approximately two orders of magnitude larger than for NO_2, the accumulation of N_2O_4 is more likely to occur when water is present on the surface.[33,45] However, it has been demonstrated that pre-adsorbed water cannot lead to the formation of N_2O_4 on γ-Al_2O_3.[23] Therefore, the formation of N_2O_4 might be related to the surface S(IV) species. In addition, the formation of N_2O_4 was also promoted by O_2. Consequently, the autoionization of N_2O_4 leads to the formation of $NO^+NO_3^-$, which can oxidize sulfite to sulfate, while $NO^+NO_3^-$ is reduced to nitrite. Lastly, nitrite is converted to nitrate and gas phase NO in an LH type or ER type mechanism. The released NO is oxidized to NO_2 and enters into the next reaction cycle. The reaction process may be as follows:

Stage 1:

$$NO_{2(g)} \leftrightarrow NO_{2(ad)}$$

$$SO_2 + MO \rightarrow MSO_3$$

Stage 2:

$$2NO_{2(ad)} \overset{S(IV)}{\underset{O_2}{\longleftrightarrow}} N_2O_{4(ad)}$$

$$N_2O_{4(ad)} \rightarrow NO^+NO_3^-$$

Stage 3:

$$NO^+NO_3^- + MSO_3 \rightarrow MSO_4 + NO^+NO_2^-$$

$$NO^+NO_2^- + MO \rightarrow 2MNO_2$$

Stage 4:

$$2MNO_2 \rightarrow MNO_3 + NO_{(g)} \quad LH$$

$$MNO_2 + NO_{2(g)} \rightarrow MNO_3 + NO_{(g)} \quad ER$$

$$2NO_{(g)} + O_{2(g)} \rightarrow 2NO_{2(g)}$$

where M represents the surface metal sites, while MO represents the surface reactive oxygen sites. These reactive oxygen species include oxygen radicals (*e.g.* O_2^- and O^-) and other coordinatively unsaturated oxygen species. However, it is difficult to

identify and confirm them in the reaction. The synergistic effect between SO_2 and NO_2 was not observed on other mineral particles (such as $CaCO_3$ and $CaSO_4$) probably attributes to the insufficient surface oxygen sites. Due to the scarcity of adsorption sites for SO_2, further reaction is forbidden. The formation of nitrite in stage 3 was not detected by spectroscopic characterization in the SO_2 and NO_2 simultaneous reaction (*e.g.* Fig. 1), probably attributes to the rapid conversion to nitrate and gaseous product of NO. It should be noted that the relative humidity (RH) in the feed gas was less than 5% RH, therefore the present study could only represent dry conditions in the atmosphere. However, water plays an important role in atmospheric chemistry. For example, the adsorbed water film on $CaCO_3$ could enhance the uptake of sulfur dioxide and nitric acid on the surface.[47] Therefore, the mechanism of synergistic reaction might change under high RH conditions, and it will be studied in future research.

4. Conclusions and atmospheric implications

A new formation pathway of sulfate in the atmosphere was proposed. The synergistic reaction between SO_2 and NO_2 on mineral oxides at ambient temperatures promoted the transformation of SO_2 to sulfate. The N_2O_4 acted as an intermediate species and oxidized sulfite to sulfate. The oxidation process was greatly promoted by the presence of O_2 and NO_2. Due to the lack of surface oxygen sites, the synergistic effect on other mineral particles, such as $CaCO_3$ and $CaSO_4$, was not observed.

The heterogeneous reaction of mixed SO_2 and NO_2 with atmospheric concentration levels (500 ppbv SO_2 and 500 ppbv NO_2) on CaO suggested the probability of this synergistic effect in the atmosphere, although longer experimental time was needed than that with higher concentration (Fig. S3, ESI†). Previous field measurement studies have suggested that sulfate is internally mixed with nitrate and mineral dust. The present study proposed a new formation pathway of the internal mixture *via* the synergistic reaction between SO_2 and NO_2 on mineral oxides. The variation in mixture state has a significant influence on the physicochemical properties of mineral oxides. The optical properties will change because sulfate does not absorb solar radiation. Therefore, direct climate forcing of the mixture will change as sulfate and nitrate have a cooling effect while mineral dust has a heating effect in the atmosphere.[6,13] Since sulfate and nitrate are hygroscopic, mineral oxides internally mixed with them can absorb more water. Their cloud condensation nuclei potential is significantly enhanced, while indirect climate forcing of particles is changed.[10] In addition, greater hygroscopicity may create an aqueous layer over the particles and therefore facilitate further adsorption and reaction of other pollutants under ambient atmospheric conditions. These results provide insight into the complex relationship between global sulfur and nitrogen circulation and atmospheric particles.

Acknowledgements

This research was financially supported by the National Natural Science Foundation of China (20937004, 50921064, and 20877084). Chang Liu also acknowledges the Science and Technology Innovation Foundation for Graduate Students of Chinese Academy of Sciences.

Notes and references

1 J. Lelieveld, P. J. Crutzen, V. Ramanathan, M. O. Andreae, C. A. M. Brenninkmeijer, T. Campos, G. R. Cass, R. R. Dickerson, H. Fischer, J. A. de Gouw, A. Hansel, A. Jefferson, D. Kley, A. T. J. de Laat, S. Lal, M. G. Lawrence, J. M. Lobert, O. L. Mayol-Bracero, A. P. Mitra, T. Novakov, S. J. Oltmans, K. A. Prather, T. Reiner, H. Rodhe, H. A. Scheeren, D. Sikka and J. Williams, *Science*, 2001, **291**, 1031–1036.
2 J. Langner and H. Rodhe, *J. Atmos. Chem.*, 1991, **13**, 225–263.
3 P. Warneck, *Chemistry of the natural atmosphere*, Academic Press, Londan, 2nd edn, 2000.
4 J. Langner, H. Rodhe, P. J. Crutzen and P. Zimmermann, *Nature*, 1992, **359**, 712–716.
5 R. J. Charlson, S. E. Schwartz, J. M. Hales, R. D. Cess, J. A. Coakley, Jr., J. E. Hansen and D. J. Hof mann, *Science*, 1992, **255**, 423–423.
6 S. K. Satheesh and K. Krishna Moorthy, *Atmos. Environ.*, 2005, **39**, 2089–2110.
7 J. Lelieveld and J. Heintzenberg, *Science*, 1992, **258**, 117–120.
8 J. T. Kiehl and B. P. Briegleb, *Science*, 1993, **260**, 311–314.
9 V. Ramanathan, P. J. Crutzen, J. T. Kiehl and D. Rosenfeld, *Science*, 2001, **294**, 2119–2124.
10 C. C. Chuang and J. E. Penner, *Tellus, Ser. B*, 1995, **47**, 566–577.
11 M. A. Tolbert, *Science*, 1994, **264**, 527–528.
12 M. E. Wise, K. J. Baustian and M. A. Tolbert, *Proc. Natl. Acad. Sci. U. S. A.*, 2010, **107**, 6693.
13 J. Haywood and O. Boucher, *Rev. Geophys.*, 2000, **38**, 513–543.
14 IPCC "IPCC Fourth Assessment Report: Working Group I Report The Physical Science Basis", 2007.
15 D. W. Gunz and M. R. Hoffmann, *Atmos. Environ.*, 1990, **24**, 1601–1633.
16 L. A. Barrie, Y. Yi, W. R. Leaitch, U. Lohmann, P. Kasibhatla, G. J. Roelofs, J. Wilson, F. Mcgovern, C. Benkovitz, M. A. Mélières, K. Law, J. Prospero, M. Kritz, D. Bergmann, C. Bridgeman, M. Chin, J. Christensen, R. Easter, J. Feichter, C. Land, A. Jeuken, E. Kjellström, D. Koch and P. Rasch, *Tellus, Ser. B*, 2001, **53**, 615–645.
17 C. R. Usher, H. Al-Hosney, S. Carlos-Cuellar and V. H. Grassian, *J. Geophys. Res., [Atmos.]*, 2002, **107**, 4713.
18 W. F. Schneider, J. Li and K. C. Hass, *J. Phys. Chem. B*, 2001, **105**, 6972–6979.
19 A. L. Goodman, P. Li, C. R. Usher and V. H. Grassian, *J. Phys. Chem. A*, 2001, **105**, 6109–6120.
20 M. Ullerstam, R. Vogt, S. Langer and E. Ljungström, *Phys. Chem. Chem. Phys.*, 2002, **4**, 4694–4699.
21 T. Ishizuka, H. Kabashima, T. Yamaguchi, K. Tanabe and H. Hattori, *Environ. Sci. Technol.*, 2000, **34**, 2799–2803.
22 M. Ullerstam, M. S. Johnson, R. Vogt and E. Ljungström, *Atmos. Chem. Phys.*, 2003, **3**, 2043–2051.
23 Q. X. Ma, Y. C. Liu and H. He, *J. Phys. Chem. A*, 2008, **112**, 6630–6635.
24 C. R. Usher, A. E. Michel and V. H. Grassian, *Chem. Rev.*, 2003, **103**, 4883–4940.
25 A. A. Davydov, *Molecular Spectroscopy of Oxide Catalyst Surfaces*, Wiley, New York, 2003.
26 M. A. Martin, J. W. Childers and R. A. Palmer, *Appl. Spectrosc.*, 1987, **41**, 120–126.
27 H. Dathe, A. Jentys, P. Haider, E. Schreier, R. Fricke and J. A. Lercher, *Phys. Chem. Chem. Phys.*, 2006, **8**, 1601–1613.
28 S. J. Hug, *J. Colloid Interface Sci.*, 1997, **188**, 415–422.
29 J. Baltrusaitis, J. Schuttlefield, J. H. Jensen and V. H. Grassian, *Phys. Chem. Chem. Phys.*, 2007, **9**, 4970–4980.
30 A. L. Goodman, E. T. Bernard and V. H. Grassian, *J. Phys. Chem. A*, 2001, **105**, 6443–6457.
31 W. S. Barney and B. J. Finlayson-Pitts, *J. Phys. Chem. A*, 2000, **104**, 171–175.
32 A. L. Goodman, G. M. Underwood and V. H. Grassian, *J. Phys. Chem. A*, 1999, **103**, 7217–7223.
33 B. J. Finlayson-Pitts, L. M. Wingen, A. L. Sumner, D. Syomin and K. A. Ramazan, *Phys. Chem. Chem. Phys.*, 2003, **5**, 223–242.
34 J. F. Liu, Y. B. Yu, Y. J. Mu and H. He, *J. Phys. Chem. B*, 2006, **110**, 3225–3230.

35 R. C. Sullivan, M. J. K. Moore, M. D. Petters, S. M. Kreidenweis, G. C. Roberts and K. A. Prather, *Atmos. Chem. Phys.*, 2009, **9**, 3303–3316.
36 G. Piazzesi, M. Elsener, O. Kröcher and A. Wokaun, *Appl. Catal., B*, 2006, **65**, 169–174.
37 G. M. Underwood, T. M. Miller and V. H. Grassian, *J. Phys. Chem. A*, 1999, **103**, 6184–6190.
38 K. Hadjiivanov and H. Knözinger, *Phys. Chem. Chem. Phys.*, 2000, **2**, 2803–2806.
39 D. Peak, R. G. Ford and D. L. Sparks, *J. Colloid Interface Sci.*, 1999, **218**, 289–299.
40 H. B. Fu, X. Wang, H. B. Wu, Y. Yin and J. M. Chen, *J. Phys. Chem. C*, 2007, **111**, 6077–6085.
41 T. Venkov, K. Hadjiivanov and D. Klissurski, *Phys. Chem. Chem. Phys.*, 2002, **4**, 2443–2448.
42 M. Ziolek, J. Kujawa, O. Saur, A. Aboulayt and J. C. Lavalley, *J. Mol. Catal. A: Chem.*, 1996, **112**, 125–132.
43 X. Y. Zhang, G. S. Zhuang, J. M. Chen, Y. Wang, X. Wang, Z. S. An and P. Zhang, *J. Phys. Chem. B*, 2006, **110**, 12588–12596.
44 C. Börensen, U. Kirchner, V. Scheer, R. Vogt and R. Zellner, *J. Phys. Chem. A*, 2000, **104**, 5036–5045.
45 C. C. Addison, *Chem. Rev.*, 1980, **80**, 21–39.
46 B. J. Finlayson-Pitts, *Phys. Chem. Chem. Phys.*, 2009, **11**, 7760–7779.
47 H. A. Al-Hosney and V. H. Grassian, *Phys. Chem. Chem. Phys.*, 2005, **7**, 1266–1276.

